MODELLING AND SIMULATION ON CAVITY COLD PLATE FOR LI-ION BATTERY THERMAL MANAGEMENT

Wang, T.[*]; Zhang, X.[*,#]; Zeng, Q. L.[**]; Jiang, S. B.[*] & Zhang, Y. N.[***]

[*] College of Mechanical and Electronic Engineering, Shandong University of Science and Technology, Qingdao, 266590, China

[**] College of Information Science and Engineering, Shandong Normal University, Jinan, 250358, China

[***] Faculty of Mechanical Engineering, Czech Technical University in Prague, Prague 6, 16000, Czech Republic

E-Mail: zhangxinmt@163.com ([#] Corresponding author)

Abstract

Recently, the safety of electric vehicles using lithium-ion batteries has received increased attention due to overheating. Cold plates can effectively enhance heat dissipation. However, given the defects of existing cold plates, such as complex structure and heavy weight, a simple cavity cold plate is designed. The effects of cold plate inlet and outlet sizes (d_2 and Δd), mass flow rate of coolant (W), and the inlet and outlet position on cell's maximum temperature and temperature difference are analysed using computational fluid dynamics (CFD) to enhance the heat dissipation capacity of the cold plate. Results show that the inlet and outlet sizes are positively correlated with the cell's maximum temperature. In addition, the cavity cold plate can satisfy the requirements of battery temperature difference by optimizing the inlet and outlet sizes and W. The cooling system of Model Z has better heat dissipation capacity than that of Model N. Conclusions obtained in the study have important reference for optimization of cavity cold plates.

(Received in November 2021, accepted in January 2022. This paper was with the authors 1 month for 1 revision.)

Key Words: Cold Plate Modelling, Thermal Simulation, Battery Thermal Management, CFD

1. INTRODUCTION

In recent years, green vehicles, such as electric vehicles (EVs), have been rapidly developing, thereby offering an important approach to solve the global problems of energy crisis and environmental degradation [1, 2]. EVs have the advantages of zero-emission [3], low noise, high efficiency, and low cost because they use clean energy as power source. However, with the growth of EVs' ownership and mileage, the safety of EV battery packs has attracted increased public attention [4, 5].

Lithium-ion (Li-ion) batteries are advantageous in terms of high energy density, long cycle life, low self-discharge rate, good stability and low pollution [6]. Thus, most energy storage devices of EVs adopt lithium-ion batteries. When Li-ion battery cell is discharged at a high rate, its temperature rises rapidly. If its temperature is extremely high, then the cell's capacity is reduced. Gas is generated inside the Li-ion battery, and the cell's body swells or smokes. In more serious cases, the battery burns or explodes, seriously endangering the users' safety [7]. In addition, when cell temperature difference is extremely large, the consistency of cell is reduced, and its service life is shortened [8]. Thus, to increase the safety and service life of Li-ion batteries, battery thermal management system (BTMS) is greatly important. A reasonable BTMS should maintain the cell temperature at 25–40 °C during charging and discharging, and the temperature difference should be controlled within 5 °C. In addition, BTMS should have the advantages of small size, low energy consumption, good stability, and economy. Therefore, reasonable optimization is necessary [9].

2. STATE OF THE ART

BTMS cooling methods mostly involve the following parts: air cooling, liquid cooling, phase change materials (PCM), and heat pipes [10]. Many scholars have studied duct and air inflow of BTMS because air cooling is advantageous in simple structure, low cost, and low weight [11, 12]. However, air cooling is rather restrictive. Air has low specific heat capacity and thermal conductivity, which is not conducive to large-scale applications. In terms of PCM, BTMSs are mainly optimized by increasing the thermal conductivity of PCM. PCM with better physical properties is selected, and the heat dissipation of PCM is enhanced [13]. However, the BTMS of PCM has high quality, high cost, and poor safety; thus, it is less practical in EVs. In all thermal management methods, heat pipe is relatively new but technologically imperfect. However, heat pipe has the advantages of small size, safety and reliability, high heat dissipation efficiency, and no energy consumption. Therefore, many scholars have applied heat pipes to heat dissipation of Li-ion batteries [14, 15]. Only by solving the problems of high cost and technical difficulty of heat pipes can heat pipes truly exert their advantages.

Liquid cooling has a better development prospect than these thermal management methods. Liquid cooling, especially cold plate cooling, has the advantages of good heat transfer efficiency, heat dissipation, safety, stability, and economy. In addition, the simulation method based on experimental data can analyse the cooling effects of BTMS [16]. The existing cold plate cooling schemes mainly use mini-channel cold plates. The heat dissipation of cold plate has been enhanced by optimizing the flow distribution inside the cold plate [17]. For example, Li et al. [18] analysed four cold plates with different internal structures for heat dissipation of prismatic batteries. However, the mini-channel cold plate is more complicated and difficult to manufacture. In addition, most cold plates are made of aluminium with good physical properties. BTMS effects can also be enhanced by changing the cold plate materials. Li et al. [19] used silicon cold plates to analyse heat dissipation of prismatic batteries. However, compared with aluminium cold plates, silicon cold plates have high cost and low strength. In terms of coolants, compared with conventional coolants, such as water, oil, and aqueous solution of ethylene glycol (EGW), more scholars have studied novel coolants, such as nanofluids, liquid metals, and phase change fluids. Huo and Rao [20] studied the impacts of nanofluids on the temperature of high-power Li-ion battery. Their results showed that the addition of nanoparticles could reduce the maximum temperature of battery, with limited impacts on temperature uniformity. Yang et al. [21] compared the effects of liquid metal cooling and water cooling on heat dissipation of Li-ion batteries with different discharge rates. Al-Zareer et al. [22] used R134a phase change fluid to perform boiling cooling on battery pack under 5 C-rate (discharge rate) discharge by modelling and simulation. Although the physical parameters of these new coolants are better, their costs are higher, and some coolants are less environmentally friendly. In addition, a number of BTMS with different cooling methods have been designed, such as BTMS combined with phase change materials and cold plates, to enhance the heat transfer and improve battery temperature uniformity [22]. Composite-heat dissipation schemes have better thermal management effects than the single-heat dissipation schemes. However, they are more complicated in structure, greater in technical difficulty, and poorer in safety and stability.

In summary, cold plate BTMS has better performance and practicability than other BTMSs. Aluminium cold plates are more cost-effective, considering heat dissipation capacity and cost of cold plates. At the same time, due to its low freezing point, the aqueous solution of ethylene glycol can expand the minimum ambient temperature range for using cold plate BTMS. Existing cold plates have complicated the internal flow channel structure to achieve better cooling effects. Although this structure can enhance the heat dissipation capacity of BTMS, they also increase the difficulty of manufacturing together with cost. In response to these

problems, a cavity cold plate for heat dissipation of Li-ion batteries is studied. The cold plate is advantageous in simple structure, small weight, and low energy consumption. When the discharge rate of pouch Li-ion battery is 4 C-rate, the effects of multiple variables on Li-ion cells are analysed.

The following parts are organized as follows. Part 3 introduces the physical model of cavity cold plate BTMS in detail. The sizes of the 3D model and specific parameters of Li-ion battery cells are provided. A heat generation model is established based on battery heat generation experimental data. The grid independence of BTMS model is tested, and the simulation setting is introduced in detail. The simulation results are discussed in detail in Part 4. Conclusions are presented in the fifth section.

3. METHODOLOGY

3.1 Physical model

Fig. 1 shows the battery cooling system of cavity cold plate. The cells in the cooling system are produced by Shandong RealForce Enterprises Co., Ltd. in China and outer surface by Al-Plastic Film. The 3D model is simplified using FLUENT17.0 for simulation. The effects of cold plate body on heat dissipation of cells' body are mainly studied. The external dimensions of cold plate are consistent with the sizes of cells. d_1 is the thickness of cold plate. d_2 is the width of inlet and outlet. Δd is the difference between d_1 and d_2.
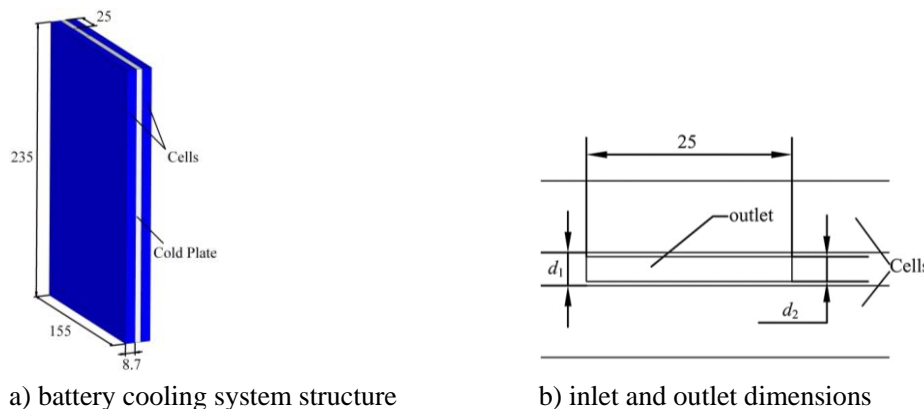

a) battery cooling system structure   b) inlet and outlet dimensions

Figure 1: Battery cooling system.

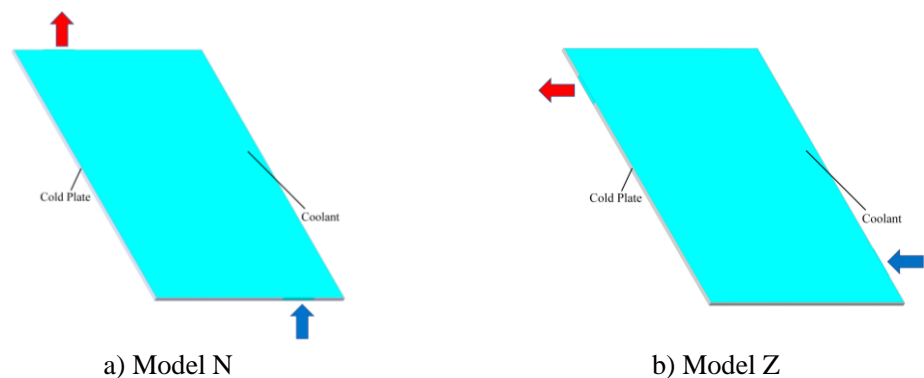a) Model N   b) Model Z

Figure 2: Flow of coolant in Model N and Model Z cold plates.

The coolant flow inside the cavity cold plate is shown in Fig. 2. The aluminium shell thickness of the cold plate is uniform at 0.5 mm, with coolant inside. The weight of the cavity cold plate is lighter than that of the other conventional cold plates with the same volume because the density of aluminium is greater than that of the coolant. The diagonally opposite inlet and

outlet of the cold plate are arranged on different sides. The layout of the inlet and outlet cold plate is changed; they are divided into two types, namely, Model N and Model Z. At the same time, by charging the inlet and outlet dimensions (d_1 and d_2), each type of cold plate is divided into seven cold plates. The specific cold plate inlet and outlet dimensions are shown in Table I.

Table I: Dimensions d_1 and d_2 of different models.

	Model 1	Model 2	Model 3	Model 4	Model 5	Model 6	Model 7
d_1 (mm)	2	3	4	5	3	4	5
d_2 (mm)	1	1	1	1	2	3	4

3.2 Heat generation model of cell with experiment data

Combined with the actual working conditions of EVs, the cell is tested for heat generation when it is discharged at 4 C-rate, and the maximum temperature of the cell is obtained. According to the experimental data, User Define Function (UDF) in FLUENT is used to define cell's heat generation density, which can be estimated in Eq. (1), as follows:

$$q = -63t + 93957.8 \tag{1}$$

where q is the average heat generation density of cell (W/m^3). t is time (s).

Fig. 3 shows the maximum temperature in the heat generation experiment and simulation, from which the relative error is lower than 2 %.
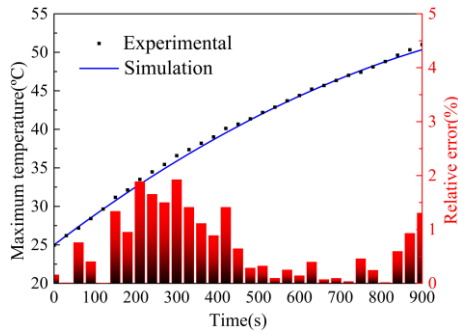

Figure 3: Comparison of cell heat generation experiment and simulation.

3.3 Meshing and grid independence test

All models are meshed by ICEM CFD 17.0. Grid independence test is carried out because the number and quality of the grids affect the simulation results, as shown in Fig. 4. The models in this study are similar; thus, the hexahedral mesh of Model N$_7$ and Model Z$_7$ is carried out. The grid number is 889248 to 6723820, and the mass flow rate (W) at cold plate inlet is 0.001 kg/s. When the number of grids is more than 5544176, the thermal transfer rate begins to stabilize in Fig. 4. Therefore, the number of all cooling system meshes is approximately 5.5 million. The quality of all meshes is greater than 0.9.
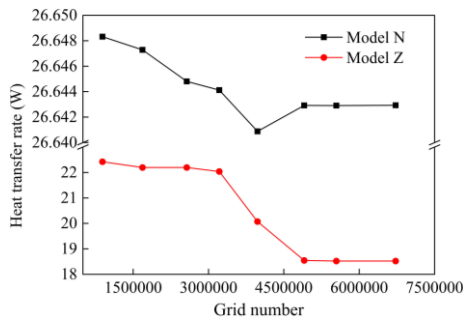

Figure 4: Model N and Model Z cold plate models grid independence test.

3.4 Simulation settings

The Reynolds numbers of all cooling systems are calculated in the range of 101.72 to 567.28. Laminar Viscous Model is selected because the Reynolds numbers (Re) of the cooling system are less than 2300. The slip of the coolant relative to inner surface of cavity cold plate and the thermal contact resistance in cooling systems are ignored. The inlet boundary type is mass flow inlet, and the outlet boundary type is outflow. The mass flow rates are set to 0.005, 0.01, 0.015, 0.02 and 0.025 kg/s. The initial temperature of the coolant is 25 °C. Cells and cold plate to air contact surfaces are set to convection thermal condition, and the heat transfer coefficient and free stream temperature to 5 W/(m²·K) and 25 °C, respectively. The thermophysical parameters of the material in simulation are shown in Table II [23].

Table II: Thermal properties of materials.

Material	Density (kg/m³)	Heat capacity (J/kg·K)	Heat conductive coefficient (W/m·K)	Dynamic viscosity (Pa·s)
50 % EGW	1071.11	3300	0.384	0.00339
Battery	1924.9	1210	0.9/2.7/2.7	-
Aluminium	2719	871	202.4	-
Al-Plastic Film	1390	460	66.6	-

4. RESULTS AND DISCUSSION

Maximum temperature (T_m) is the maximum temperature value of cell at a certain moment, and the highest maximum temperature (T_H) is the highest value of the 30 maximum temperatures in a set of simulation data. The temperature difference (ΔT) is the difference between the maximum temperature and the minimum temperature of cell at a certain moment. Accordingly, the maximum temperature difference (ΔT_m) is the highest value of the 30 temperature differences in a set of simulation data.

4.1 Effects of cold plate inlet and outlet sizes on temperature

According to Fig. 5, regardless of the cold plate size, the T_m of cell increases initially and then decreases. T_m is reached at a certain discharge time and is related to heat generation rate.
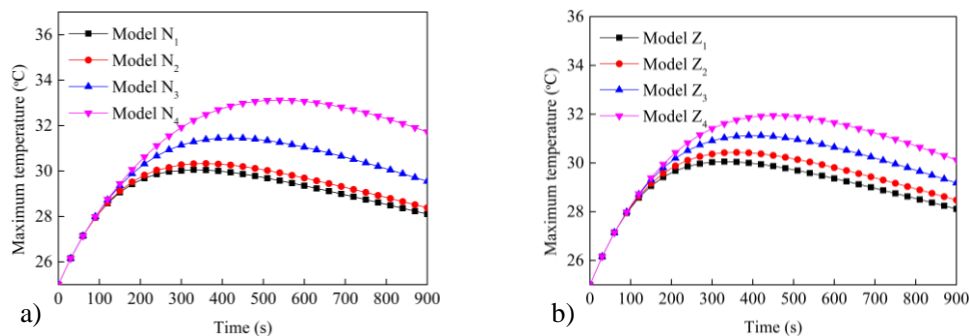

Figure 5: T_m of cells in Models N and Z with d_2 of 1 mm.

In Fig. 5 a, the T_m of cells in N_1 is 30.1 °C at 330 s when W is 0.01 kg/s. The cells in N_2 reach T_m of 30.3 °C at 360 s, with an increase in 0.2 °C, compared with Model N_1. When d_1 increases to 4 mm, the cells in N_3 reach T_m of 31.5 °C at 420 s, with an increase of 1.2 °C compared with Model N_2. The cells in Model N_4 reach T_m of 33.1 °C at 540 s, 1.6 °C higher than that of Model N_3. Evidently, T_m increases gradually with the increase in Δd, and the time for reaching T_m is gradually delayed. T_m in Model N appears at the cell's corners in Fig. 6. The

figure shows that as the thickness of cavity cold plate increases, the coolant flow at the four cold plate corners slows down. All T_m is below 34 °C.

In Fig. 5 b, when W is 0.01 kg/s, T_m in Model Z gradually increases with the increase in Δd. In addition, the time to reach T_m is gradually delayed. For instance, when W is 0.01 kg/s, the cells in Z_1 reach a T_m of 30.1 °C at 330 s, and the cells in Z_2 reach a T_m of 30.4 °C at 360 s. The cells in Z_4 reach a T_m of 31.9 °C at 450 s. All T_m is less than 32 °C. With the increase in Δd, the reason for the increase in T_m of Model Z is consistent with that in Model N.

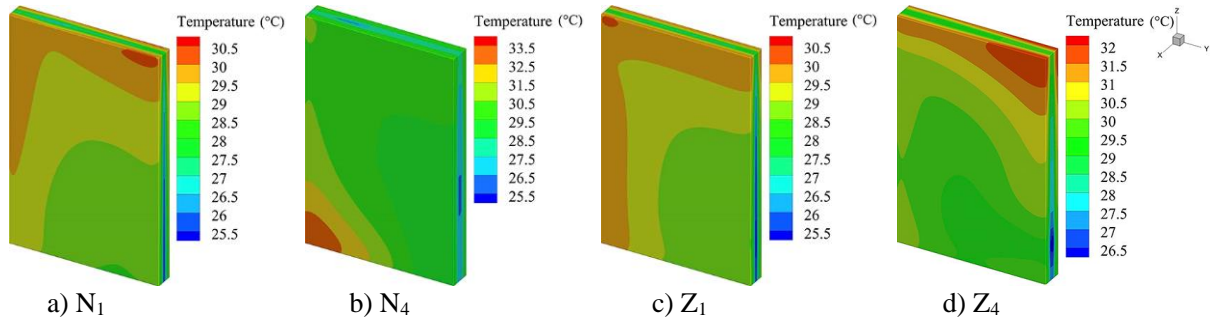| a) N_1 | b) N_4 | c) Z_1 | d) Z_4 |

Figure 6: Temperature contours of different cooling system types with W of 0.01 kg/s.

In Fig. 7, when W is 0.01 kg/s, the cells in N_5 reach a T_m of 30.3 °C at 360 s, 0.2 °C higher than that in N_1. The cells in N_6 reach a T_m of 30.6 °C at 360 s, 0.3 °C higher than that in N_5. The cells in N_7 reach a T_m of 30.9 °C at 420 s, 0.3 °C higher than that in N_5. In summary, when W is 0.01 kg/s, with the increase in d_2, T_m in Model N gradually increases. And the time to reach T_m is gradually delayed. The increase in T_m is 0.2–0.3 °C, because the increase in d_2 reduces the flow velocity at the cold plate inlet in the same W. The decrease in internal fluidity of the coolant in the cavity cold plate gradually increases the heat accumulation at the edge of the battery and T_m. In Fig. 7 b, when W is 0.01 kg/s, the T_m of cells in Model Z gradually increases with the increase in d_2. The time to reach T_m is gradually delayed, and T_m is below 32 °C.
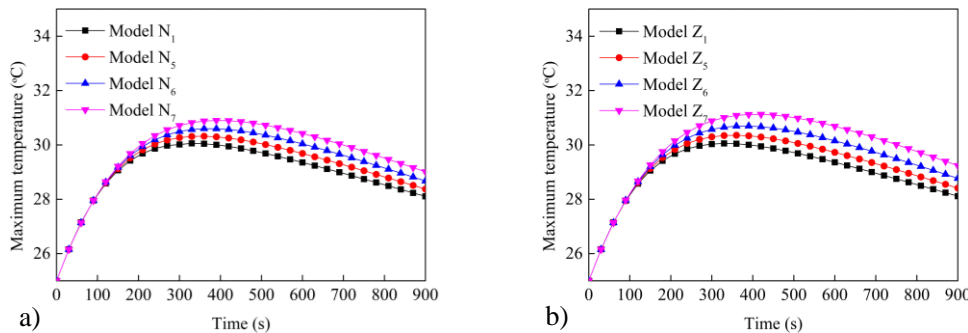

Figure 7: T_m of cells in Models N and Z with Δd of 1 mm.

ΔT shares similar rules with T_m, as shown in Fig. 8. When W is 0.01 kg/s, the ΔT_m of the cells in N_1 is 4.4 °C, and the ΔT_m in N_2 is 4.6 °C; the increase is 0.2 °C. The ΔT_m in N_3 is 5.4 °C, and the increase is 0.8 °C. ΔT_m in N_4 is 6.7 °C, and the increase is 1.3 °C. In summary, the ΔT_m of the cells gradually increases with the increase in Δd, and the increase is gradual. The reasons of ΔT rules are the same as those of T_m. In Fig. 8 b, the ΔT_m of cells in Model Z gradually increases with the increase in Δd, which increases significantly with the increase in Δd. For example, when W is 0.02 kg/s, the ΔT_m in Z_1 is 3.7 °C, and that in Z_2 is 4.2 °C, with the increase of 0.5 °C. The ΔT_m in Z_3 is 5.0 °C, and the increase is 0.8 °C. The ΔT_m in Z_4 is 6.4 °C, and the increase is 1.4 °C. The reasons for the rules are the same as those of Model N.

In summary, the rules of the cells' ΔT agree with those of T_m, that is, the increase in ΔT is gradual with the increase in Δd. When d_2 is 1 mm and Δd is less than or equal to 2 mm, ΔT_m is

less than 5 °C in Model N and Model Z, thereby satisfying the requirements of battery heat dissipation.
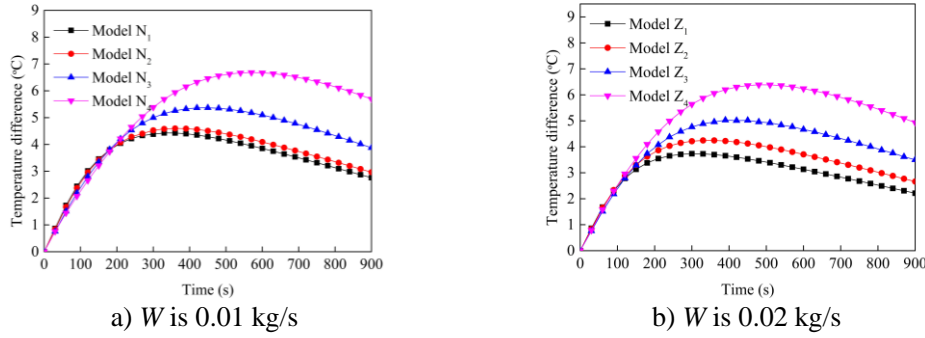

a) W is 0.01 kg/s

b) W is 0.02 kg/s

Figure 8: ΔT of cells in Models N and Z with d_2 of 1 mm.

In Fig. 9, when W is 0.01 kg/s, the ΔT_m values of cells in N_5, N_6, and N_7 are 4.6 °C, 4.8 °C, and 5.0 °C, respectively. That is, with the increase in d_2, ΔT_m gradually increases, and the increase is 0.2 °C. However, when Δd is 1 mm and W is 0.01 kg/s, the ΔT_m in all Model N is less than 5 °C. In addition, except for N_7, the cells' ΔT_m in other cooling systems is less than 5 °C, thereby satisfying the requirements of BTMS. In Fig. 9 b, when W is 0.01 kg/s, ΔT_m values of cells in Z_1, Z_5, Z_6, and Z_7 are 4.4 °C, 4.7 °C, 4.9 °C, and 5.2 °C, respectively. The results show that with the increase in d_2, ΔT_m in Model Z gradually increases by 0.2–0.3 °C. However, when W is 0.01 kg/s, ΔT_m of cells in Model Z with d_2 less than 4 mm is less than 5 °C.

In summary, although the ΔT_m of cells in Model N and Model Z gradually increases with the increase in d_2, the increase of ΔT is gradual with Δd of 1 mm. Both system types can control ΔT to satisfy the thermal management requirements of less than 5 °C.
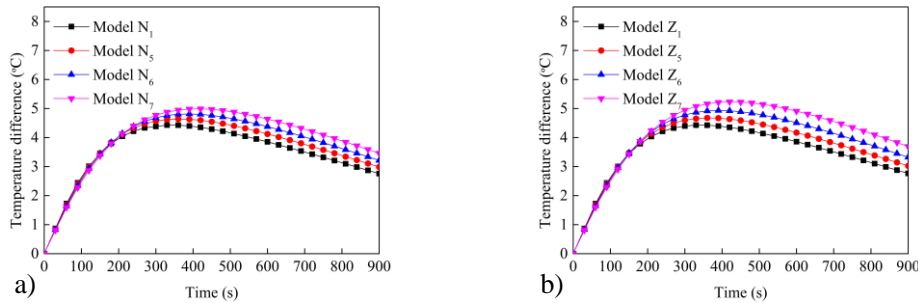

a)

b)

Figure 9: ΔT in Models N and Z with Δd of 1 mm.

4.2 Effects of coolant mass flow rate on temperature

In Fig. 10, when W is 0.005 and 0.01 kg/s, T_m in Model N gradually increases with the increase in Δd. The increase in temperature with W of 0.01 kg/s is greater than that with W of 0.005 kg/s. When Δd increases to 4 mm (N_4), T_H with W of 0.005 kg/s is 32.0 °C, which is 1.1 °C lower than that with W of 0.01 kg/s. In Fig. 11, the flow velocity with W of 0.01 kg/s in the area near the inlet and outlet is higher than that with W of 0.005 kg/s in N_4. The area with higher flow velocity is more concentrated. The flow in the inner area of the lower left corner is worse. This condition causes heat to accumulate, and the cells' T_H is in this region. When W is 0.015, 0.02, and 0.025 kg/s, T_H in Model N initially increases and then decreases with the increase in Δd. The extreme points of the T_H curves of the three conditions appear at the Δd of 3 mm (N_3). In Model N, when d_2 is 1 mm, the slope of the T_H curve is different at different d_1 ranges. Thus, in different models, the order of T_H under different W is different. For example, in N_2, the T_H is 31.5 °C when W is 0.005 kg/s; in N_3, T_H is 32.7 °C when W is 0.015 kg/s; in N_4, the cells reach T_H when W is 0.01 kg/s. The inlet and outlet with d_2 of 1 mm are small, and the flow velocity

of the coolant varies greatly with different W values. In addition, the flow field inside the cavity cold plate is more different. At the same time, the Δd of the cavity cold plate increases. Therefore, the thickness of the fluid domain increases, thereby further increasing the difference in flow field. However, when d_2 is 1 mm, the T_H of cells in Model N is less than 34 °C for a different W.
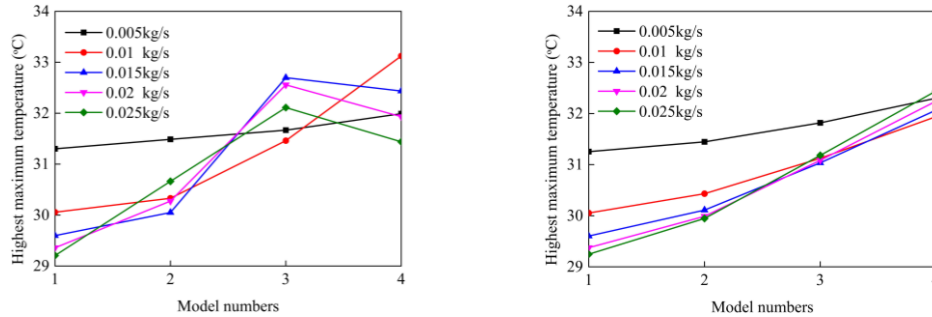

Figure 10: The cells T_H with different W in Models N and Z with d_2 of 1 mm, Model N on the left and Model Z on the right.

a) N_4, W is 0.005 kg/s   b) N_4, W is 0.01 kg/s   c) Z_3, W is 0.015 kg/s   d) Z_3, W is 0.025 kg/s

Figure 11: Slices of flow velocity contours in cavity cold plate under different mass flow rates.

In Model Z, when d_2 is 1 mm, the T_H of cells gradually increases with the increase in Δd. When W is 0.005 kg/s, it increases from 31.3 °C in Z_1 to 32.3 °C in Z_4, with an increase of 1 °C. Similarly, when W is 0.015 kg/s, the increase is 2.5 °C; when W is 0.025 kg/s, the increase is 3.2 °C. In summary, the increase in T_H gradually increases with the increase in W. The reason is that when W increases, the flow velocity of the coolant at inlet and outlet in Model Z increases, and the higher flow velocity area near the inlet and outlet is more concentrated. In addition, the thickness of the fluid domain increases, and the flow velocity at the corners away from the inlet and outlet decreases. Therefore, the temperature increases at that position. Moreover, the slope of the curves gradually increases with the increase in W. As a result, the order of T_H at different W values and Model Z is different.

Fig. 12 shows the effects of different mass flow rates on the cells' T_m in Model N and Model Z when Δd is 1 mm. In Model N, when W is 0.005 kg/s, T_H increases from 31.3 °C in N_1 to 31.9 °C in N_7, with an increase of 0.6 °C. When W is 0.01 kg/s, it increases by 0.8 °C from N_1 to N_7. When W is 0.015 kg/s, it increases by 1.6 °C from N_1 to N_7. In addition, when W is 0.02 and 0.025 kg/s, it increases by 2.4 °C and 3.3 °C, respectively. Evidently, with the increase in the mass flow rate at the cold plate inlet, the increase in T_H from N_1 to N_7 is gradual. Therefore, the slopes of the curves gradually increase with the increase in W. In N_1, with the increase in W, the T_H gradually decreases. The increase in T_H is gradual with the increase in W. Thus, W with the highest temperature is different for different Model N.

In Model Z, when W is 0.005, 0.01, 0.015, 0.02, and 0.025 kg/s, the increase in T_H is 0.6 °C, 1.0 °C, 1.3 °C, 1.5 °C, and 1.8 °C, respectively. The T_H of cells gradually decreases with the increase in W, but the reduction gradually decreases.
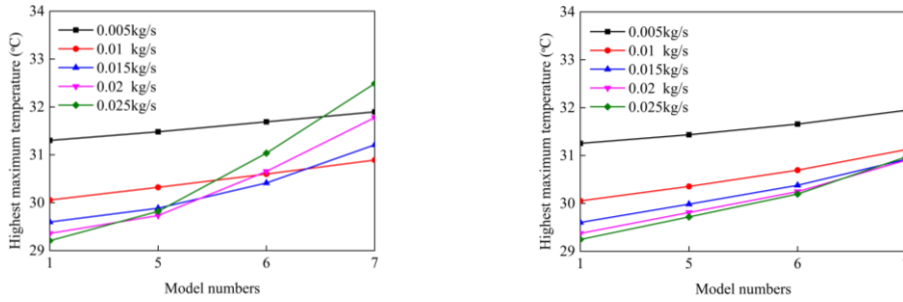
Figure 12: T_H with different W in Models N and Z with Δd of 1 mm, Model N on the left and Model Z on the right.

In Fig. 13, the rules of ΔT_m are related to those of T_H. In Model N, when W is 0.005 kg/s, the ΔT_m of cells in the four Models of N is greater than 5 °C. When W is greater than or equal to 0.01 kg/s, the ΔT_m in N_1 and N_2 is less than 5 °C, thereby satisfying the requirements of battery cooling systems. However, when Δd is increased to 3 and 4 mm (N_3 and N_4), ΔT_m is greater than 5 °C with different W. In Model Z, the rules of ΔT_m are the same as T_H. When W increases, the slope of the curves gradually increases. Similarly, when W is 0.005 kg/s, the ΔT_m in the four Models of Z is greater than 5 °C. In Z_1 and Z_2, when W is greater than or equal to 0.01 kg/s, they are less than 5 °C. In Z_3, when W is 0.01, 0.015, and 0.02 kg/s, ΔT_m is less than 5 °C. However, when W is 0.025 kg/s, ΔT_m is 5.1 °C. In Z_4, it is greater than 5 °C at any W.
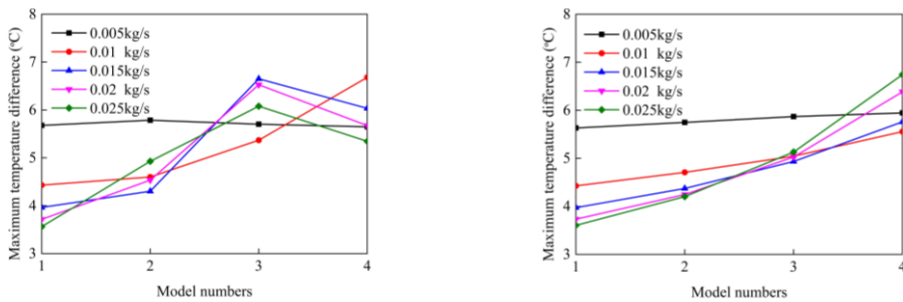

Figure 13: ΔT_m of cells with different W in Models N and Z with d_2 of 1 mm, Model N on the left and Model Z on the right.

Fig. 14 shows the effects of different mass flow rates on ΔT_m in Model N and Model Z when Δd is 1 mm. In Model N, when W is 0.005 kg/s, those in Model N with Δd of 1 mm are greater than 5 °C. However, when W is 0.01 kg/s, ΔT_m in all Models of N with Δd of 1 mm is less than 5 °C. When W is 0.015 and 0.02 kg/s and d_2 is less than or equal to 3 mm (N_1, N_5, and N_6), they are less than 5 °C. When W is 0.025 kg/s and d_2 is less than or equal to 2 mm (N_1 and N_5), ΔT_m is less than 5 °C. Similarly, in Model Z, when W is 0.005 kg/s, the ΔT_m in Model Z with Δd of 1 mm is greater than 5 °C. When W is 0.01 kg/s, Z_7 is also greater than 5 °C. However, with a different W value, the other ΔT_m in Model Z with Δd of 1 mm is less than 5 °C.
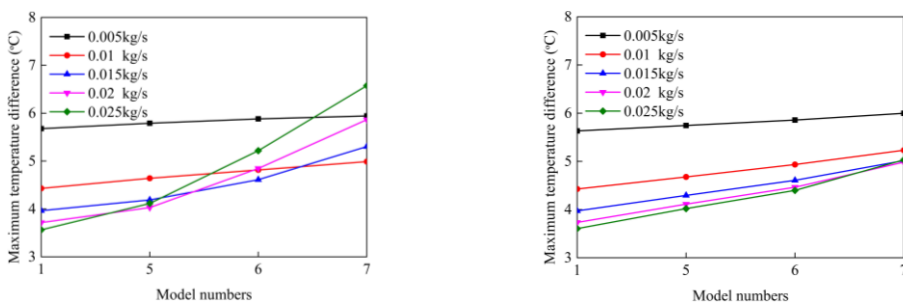

Figure 14: ΔT_m of cells with different W in Models N and Z with Δd of 1 mm, Model N on the left and Model Z on the right.

4.3 Effects of inlet and outlet positions on temperature

By combining W with different model types, two data groups of 35 T_m and ΔT_m in each group are generated, as shown in Figs. 15 and 16, respectively.

Fig. 15 shows the radars of T_H of the cells in the cavity cold plate cooling system of Model N and Model Z. Fig. 15 a shows that in Model N, when W is 0.01 kg/s, T_H (33.1 °C) appears in N_4 (d_2 is 1 mm). When W is 0.025 kg/s, the lowest T_m is 29.2 °C, which appears in N_1. In addition, the T_H exceeding 32.5 °C in Model N appears in N_3 and N_4 (d_2 is 1 mm). In Fig. 15 b, when W is 0.025 kg/s, the T_H is 32.4 °C in Z_4 (d_2 is 1 mm), and the lowest T_m 29.2 °C appears in Z_1. The T_H exceeding 32 °C in Model Z appears in Z_4. When the thickness of the cold plate is the same, the temperature curve circles with Δd of 1 mm are closer to the centre point of the radar chart than that with d_2 of 1 mm. In addition, by analysing all T_H values in Model N and Model Z, the number of cases that T_H of different cold plate types appear in different temperature ranges in Table III is obtained. In Table III, compared with Model N, the T_H in Model Z has a lower temperature range and is not higher than 33 °C.
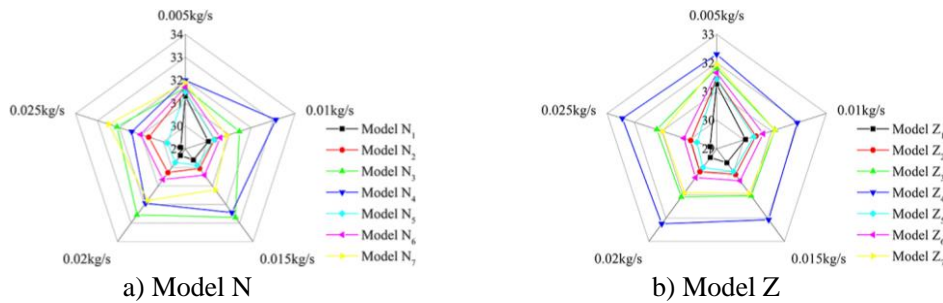

a) Model N   b) Model Z

Figure 15: Comparison of T_H in Models N and Z.

Table III: The number of cases with T_H in different temperature ranges for different cold plate types.

Temperature range (°C)	Model N	Model Z
29-30	6	8
30-31	10	11
31-32	13	12
32-33	5	4
33-34	1	-

Fig. 16 shows radars of ΔT_m in Model N and Model Z. ΔT_m rules are similar to that of T_H because ΔT_m is affected by T_H. In Fig. 16 a, ΔT_m is greater than 6 °C in N_3, N_4, and N_7 cooling systems. When W is 0.01 kg/s, ΔT_m 6.7 °C appears in N_4 (d_2 is 1 mm). When W is 0.025 kg/s, the lowest ΔT_m 3.6 °C appears in N_1. In Fig. 16 b, only in Z_4, ΔT_m exceeds 6 °C. When W is 0.025 kg/s, ΔT_m is 6.7 °C. In Z_1, when W is 0.025 kg/s, the lowest ΔT_m is 3.6 °C. Statistics show that, in Model N and Model Z, 16 and 18 cases, respectively, are required to obtain ΔT_m of less than 5 °C. Similarly, when the cavity cold plate has the same thickness, the ΔT curve circles with Δd of 1 mm are closer to the radar chart centre point than that with d_2 of 1 mm.
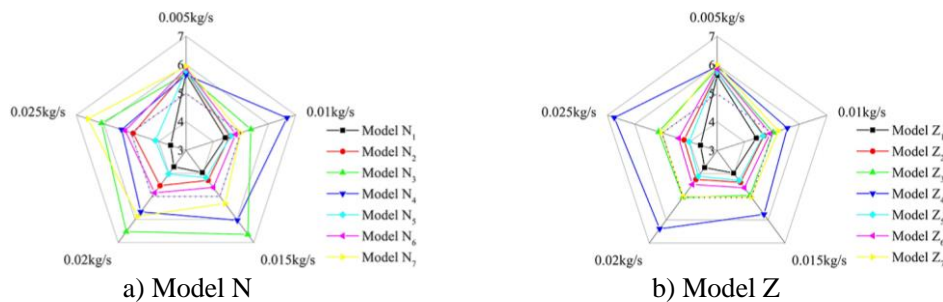

a) Model N   b) Model Z

Figure 16: Comparison of ΔT_m in Models N and Z.

5. CONCLUSION

According to the experimental data of pouch Li-ion battery heat generation, an equivalent model of battery heat generation is established. The effects of inlet and outlet dimensions (d_2 and Δd), coolant mass flow rate (W), and inlet and outlet position (Model N and Model Z) on the maximum temperature (T_m) and temperature difference (ΔT) of cells are studied using FLUENT 17.0. The conclusions are as follows:

(1) Inlet and outlet dimensions of cavity cold plate are positively correlated with T_m of cells. Under the same W, a change in d_2 or Δd can control ΔT_m within 5 °C.

(2) In Model N_1 and Model Z_1, ΔT_m gradually decreases with the increase in W, but the decrease gradually reduces. By controlling inlet and outlet sizes and W, various cases can be achieved to satisfy the ΔT of less than 5 °C.

(3) Through comprehensive analysis of Model N and Model Z, Model Z cooling system can better control the maximum temperature and ΔT of cells in a reasonable range than Model N. At the same time, the cavity cold plate with inlet dimension Δd of 1 mm has a better heat dissipation capacity than that of d_2 of 1 mm.

In summary, a reasonable design of cavity cold plate and selection of coolant mass flow rate can satisfy the thermal management requirements of pouch Li-ion battery for vehicles. This research guides the design of cold plate.

ACKNOWLEDGEMENT

REFERENCES

[1] Akhoundzadeh, M. H.; Raahemifar, K.; Panchal, S.; Samadani, E.; Haghi, E.; Fraser, R.; Fowler, M. (2019). A conceptualized hydrail powertrain: a case study of the Union Pearson Express route, *World Electric Vehicle Journal*, Vol. 10, No. 2, Paper 32, 14 pages, doi:10.3390/wevj10020032

[2] Liu, S.; Gong, D. (2014). Modelling and simulation on recycling of electric vehicle batteries-using agent approach, *International Journal of Simulation Modelling*, Vol. 13, No. 1, 79-92, doi:10.2507/IJSIMM13(1)CO1

[3] Park, S. H.; Park, J.; Ryou, M.-H.; Lee, Y. M. (2020). Sensitivity of power of lithium-ion batteries to temperature: a case study using cylindrical- and pouch-type cells, *Journal of Power Sources*, Vol. 465, Paper 228238, 7 pages, doi:10.1016/j.jpowsour.2020.228238

[4] Huang, Z. H.; Zhao, C. P.; Li, H.; Peng, W.; Zhang, Z.; Wang, Q. (2020). Experimental study on thermal runaway and its propagation in the large format lithium ion battery module with two electrical connection modes, *Energy*, Vol. 205, Paper 117906, 16 pages, doi:10.1016/j.energy.2020.117906

[5] Lv, Y.; Liu, G.; Zhang, G.; Yang, X. (2020). A novel thermal management structure using serpentine phase change material coupled with forced air convection for cylindrical battery modules, *Journal of Power Sources*, Vol. 468, Paper 228398, 9 pages, doi:10.1016/j.jpowsour.2020.228398

[6] Xie, Y.; He, X.; Li, W.; Zhang, Y.; Dan, D.; Lee, K.; Liu, J. (2020). A novel electro-thermal coupled model of lithium-ion pouch battery covering heat generation distribution and tab thermal behaviours, *International Journal of Energy Research*, Vol. 44, No. 14, 11725-11741, doi:10.1002/er.5803

[7] Cen, J.; Jiang, F. (2020). Li-ion power battery temperature control by a battery thermal management and vehicle cabin air conditioning integrated system, *Energy for Sustainable Development*, Vol. 57, 141-148, doi:10.1016/j.esd.2020.06.004

[8] Karimi, D.; Behi, H.; Jaguemont, J.; Sokkeh, M. A.; Kalogiannis, T.; Hosen, M. S.; Berecibar, M.; van Mierlo, J. (2020). Thermal performance enhancement of phase change material using aluminum-mesh grid foil for lithium-capacitor modules, *Journal of Energy Storage*, Vol. 30, Paper 101508, 12 pages, doi:10.1016/j.est.2020.101508

[9] Saw, L. H.; Poon, H. M.; Thiam, H. S.; Cai, Z. S.; Chong, W. T.; Pambudi, N. A.; King, Y. J. (2018). Novel thermal management system using mist cooling for lithium-ion battery packs, *Applied Energy*, Vol. 223, 146-158, doi:10.1016/j.apenergy.2018.04.042

[10] Wang, F. X.; Cao, J. H.; Ling, Z. Y.; Zhang, Z. G.; Fang, X. M. (2020). Experimental and simulative investigations on a phase change material nano-emulsion-based liquid cooling thermal management system for a lithium-ion battery pack, *Energy*, Vol. 207, Paper 118215, 11 pages, doi:10.1016/j.energy.2020.118215

[11] Ni, P. Y.; Wang, X. L. (2020). Temperature field and temperature difference of a battery package for a hybrid car, *Case Studies in Thermal Engineering*, Vol. 20, Paper 100646, 8 pages, doi:10.1016/j.csite.2020.100646

[12] Cho, G. Y.; Choi, J. W.; Park, J. H.; Cha, S. W. (2014). Transient modeling and validation of lithium ion battery pack with air cooled thermal management system for electric vehicles, *International Journal of Automotive Technology*, Vol. 15, No. 5, 795-803, doi:10.1007/s12239-014-0083-x

[13] Xiao, C. R.; Zhang, G. Q.; Li, Z. H.; Yang, X. Q. (2020). Custom design of solid-solid phase change material with ultra-high thermal stability for battery thermal management, *Journal of Materials Chemistry A*, Vol. 8, No. 29, 14624-14633, doi:10.1039/d0ta05247g

[14] Putra, N.; Ariantara, B.; Pamungkas, R. A. (2016). Experimental investigation on performance of lithium-ion battery thermal management system using flat plate loop heat pipe for electric vehicle application, *Applied Thermal Engineering*, Vol. 99, 784-789, doi:10.1016/j.applthermaleng.2016.01.123

[15] Wu, W. X.; Yang, X. Q.; Zhang, G. Q.; Chen, K.; Wang, S. F. (2017). Experimental investigation on the thermal performance of heat pipe-assisted phase change material based battery thermal management system, *Energy Conversion and Management*, Vol. 138, 486-492, doi:10.1016/j.enconman.2017.02.022

[16] Panchal, S.; Khasow, R.; Dincer, I.; Agelin-Chaab, M.; Fraser, R.; Fowler, M. (2017). Numerical modeling and experimental investigation of a prismatic battery subjected to water cooling, *Numerical Heat Transfer, Part A: Applications*, Vol. 71, No. 6, 626-637, doi:10.1080/10407782.2016.1277938

[17] Fang, Y. D.; Shen, J. L.; Zhu, Y.; Ye, F.; Li, K.; Su, L. (2021). Investigation on the transient thermal performance of a mini-channel cold plate for battery thermal management, *Journal of Thermal Science*, Vol. 30, No. 3, 914-925, doi:10.1007/s11630-020-1280-8

[18] Li, M.; Wang, J. C.; Guo, Q.; Li, Y.; Xue, Q. F.; Qin, G. H. (2020). Numerical analysis of cooling plates with different structures for electric vehicle battery thermal management systems, *Journal of Energy Engineering*, Vol. 146, No. 4, Paper 04020037, 10 pages, doi:10.1061/(ASCE)EY.1943-7897.0000648

[19] Li, X. X.; Zhou, D. Q.; Zhang, G. Q.; Wang, C.; Lin, R. H.; Zhong, Z. D. (2019). Experimental investigation of the thermal performance of silicon cold plate for battery thermal management system, *Applied Thermal Engineering*, Vol. 155, 331-340, doi:10.1016/j.applthermaleng.2019.04.007

[20] Huo, Y. T.; Rao, Z. H. (2015). The numerical investigation of nanofluid based cylinder battery thermal management using lattice Boltzmann method, *International Journal of Heat and Mass Transfer*, Vol. 91, 374-384, doi:10.1016/j.ijheatmasstransfer.2015.07.128

[21] Yang, X.-H.; Tan, S.-C.; Liu, J. (2016). Thermal management of Li-ion battery with liquid metal, *Energy Conversion and Management*, Vol. 117, 577-585, doi:10.1016/j.enconman.2016.03.054

[22] Al-Zareer, M.; Dincer, I.; Rosen, M. A. (2018). Heat and mass transfer modeling and assessment of a new battery cooling system, *International Journal of Heat and Mass Transfer*, Vol. 126, Part A, 765-778, doi:10.1016/j.ijheatmasstransfer.2018.04.157

[23] Zhang, X.; Wang, T.; Jiang, S. B.; Xu, H. G.; Zhang, Y. N. (2018). Modelling and simulation of pouch lithium-ion battery thermal management using cold plate, *International Journal of Simulation Modelling*, Vol. 17, No. 3, 498-511, doi:10.2507/IJSIMM17(3)449